

Gas-phase formation of fullerene/9-hydroxyfluorene cluster cations

Yin Wu,¹ Xiaoyi Hu,² Junfeng Zhen,^{3*} Xuejuan Yang,^{1†}

¹ Hunan Key Laboratory for Stellar and Interstellar Physics, and School of Physics and Optoelectronics, Xiangtan University, Hunan 411105, China

² Department of Chemical Physics, University of Science and Technology of China, 96 Jinzhai RD., Hefei, Anhui 230026, China

³ Institute of Deep Space Sciences, Deep Space Exploration Laboratory, Hefei 230026, China

28 May 2024

ABSTRACT

In interstellar environment, fullerene species readily react with large molecules (e.g., PAHs and their derivatives) in the gas phase, which may be the formation route of carbon dust grains in space. In this work, the gas-phase ion-molecule collision reaction between fullerene cations (C_n^+ , $n=32, 34, \dots, 60$) and functionalized PAH molecules (9-hydroxyfluorene, $C_{13}H_{10}O$) are investigated both experimentally and theoretically. The experimental results show that fullerene/9-hydroxyfluorene cluster cations are efficiently formed, leading to a series of large fullerene/9-hydroxyfluorene cluster cations (e.g., $[(C_{13}H_{10}O)C_{60}]^+$, $[(C_{13}H_{10}O)_3C_{58}]^+$, and $[(C_{26}H_{18}O)(C_{13}H_{10}O)_2C_{48}]^+$). The binding energies and optimized structures of typical fullerene/9-hydroxyfluorene cluster cations were calculated. The bonding ability plays a decisive role in the cluster formation processes. The reaction surfaces, modes and combination reaction sites can result in different binding energies, which represent the relative chemical reactivity. Therefore, the geometry and composition of fullerene/9-hydroxyfluorene cluster cations are complicated. In addition, there is an enhanced chemical reactivity for smaller fullerene cations, which is mainly attributed to the newly formed deformed carbon rings (e.g., 7 C-ring). As part of the coevolution network of interstellar fullerene chemistry, our results suggest that ion-molecule collision reactions contribute to the formation of various fullerene/9-hydroxyfluorene cluster cations in the ISM, providing insights into different chemical reactivity caused by oxygenated functional groups (e.g., hydroxyl, OH, or ether, C-O-C) on the cluster formations.

Key words:

astrochemistry—methods: laboratory: molecular—ultraviolet: ISM—ISM: molecules—ISM: evolution—molecular processes

1 INTRODUCTION

In the interstellar medium (ISM) of galaxies, polycyclic aromatic hydrocarbon (PAH) molecules and their derivatives generally contribute to the infrared (IR) broadband features at 3.3, 6.2, 7.7, 8.6, and 11.2 μm (e.g. Sellgren 1984; Allamandola et al. 1989; Puget & Leger 1989). These molecules have been reported to be abundant and contain about 10% of the elemental carbon in space, and they play a significant role in the ionization and energy balance of ISM (Tielens 2013, and reference therein). Subsequently, they are further processed for hundreds of millions of years in the harsh environment of the ISM, in which various types of functional groups may be acquired, leading to functionalized PAHs, such as methyl ($-\text{CH}_3$), vinyl ($-\text{CHCH}_2$), methoxy ($-\text{OCH}_3$), amino ($-\text{NH}_2$), cyano and isocyno ($-\text{CN}$, $-\text{NC}$), acid ($-\text{COOH}$), and hydroxyl ($-\text{OH}$) (Hollenbach & Tielens 1999; Bernstein et al. 2002; Al-

lamandola 2011). Recently, two nitrile-group-functionalized PAHs, 1- and 2-cyano naphthalene, were detected in the ISM. Both bicyclic ring PAH molecules were observed and confirmed in the TMC-1 molecular cloud (McGuire et al. 2021).

It has been reported that fullerenes, C_{60} and C_{70} , also exist in space according to the IR spectra of circumstellar and interstellar sources (Cami et al. 2010; Sellgren et al. 2010). Extensive experimental and theoretical investigations reveal that fullerene molecules may be formed by large PAHs through photochemical evolution in interstellar environments (Berné & Tielens 2012; Zhen et al. 2014; Omont 2016; Candian et al. 2019). Moreover, several near-IR diffuse interstellar bands (DIBs) were linked to the electronic transitions of fullerene cation C_{60}^+ (Campbell et al. 2015; Walker et al. 2015; Cordiner et al. 2017), providing new insights into understanding the chemical complexity of ISM (Campbell & Maier 2018; Cordiner et al. 2019). The stability of fullerenes with large C-atom counts ($n=44, 45, \dots, 70$) was theoretically investigated, which suggested that smaller fullerenes with C-

* E-mail: jfzhen@ustc.edu.cn

† E-mail: xjyang@xtu.edu.cn

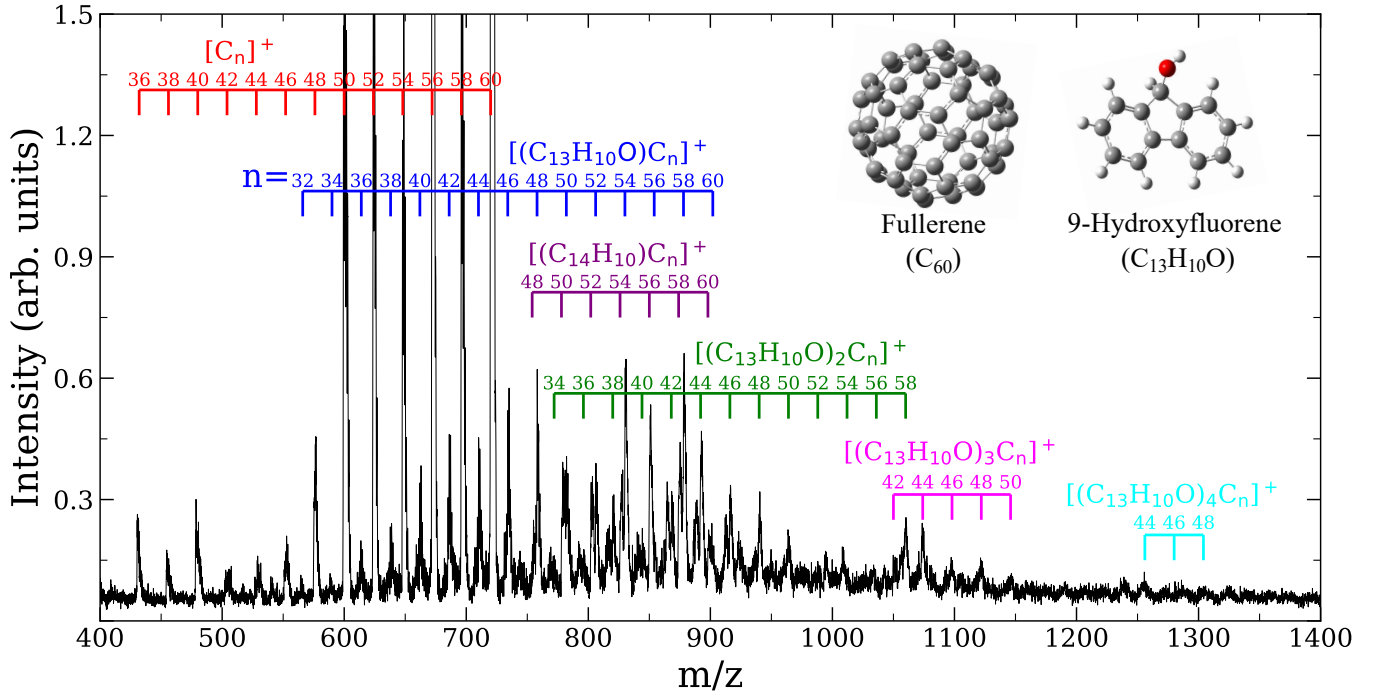


Figure 1. The resulting mass spectrum of fullerene/9-hydroxyfluorene cluster cations. The structures of fullerene (C_{60}) and 9-hydroxyfluorene ($C_{13}H_{10}O$) are shown. The cation cluster series ($[(C_{13}H_{10}O)_{1-4}C_n]^+$) and their mass fragments are labeled, together with fullerene/anthracene cluster cations ($[(C_{14}H_{10})C_n]^+$) resulting from contamination.

atom counts of 56, 50, and 44 possibly exist in astrophysical sources (Candian et al. 2019).

In interstellar space where PAH and fullerene molecules coexist, fullerene/PAH adducts and their associated derivate clusters may be formed through ion-molecule reactions in the gas phase, resulting in the existence of large fullerene/PAH derived clusters (Petrie & Bohme 1993; Dunk et al. 2013; García-Hernández et al. 2013; Böhme 2016; Omont 2016; Zhen et al. 2019b). Furthermore, the size of some large fullerene/PAH clusters can fall into the range of a few nanometers, and when they are condensed, they may be further incorporated into cosmic grains (Zhen et al. 2019b; Hu et al. 2021a). Therefore, studies on the formation of fullerene/PAHs clusters can offer a possible formation pathway for the grains, and provide insight for understanding the evolution of carbon-rich molecules (Gavilan Marin et al. 2020).

The ionization or chemical states of interstellar PAHs, fullerenes, and their derivatives are expected to be significantly affected by their chemical-physical environments (Bakes & Tielens 1994; Le Page et al. 2001). To understand the chemical characteristics of interstellar fullerenes and PAHs, the differential chemical reactivity of fullerenes and various types of PAHs are needed to investigate, e.g., PAHs with substituted functional groups (Böhme 2016; Zhen et al. 2019a,b; Hu et al. 2021a,b).

To understand the reaction between fullerene cations and oxygenated groups substituted PAH molecules, and further investigate the coevolution network of interstellar fullerene chemistry (Tielens 2013; Omont 2016), in this work, we present an exploration study of the chemical reactivity of the fullerene cations (C_n^+ , $n=32, 34, \dots, 60$) with 9-hydroxyfluorene ($C_{13}H_{10}O$, 24 atoms, 182 amu). Furthermore, to investigate the formation mechanism of fullerene/9-

hydroxyfluorene cluster cations, the experimental results are illustrated together with the results of the theoretical chemistry calculation.

The molecule 9-hydroxyfluorene, the structure of which is shown in the top right corner of Fig 1, is selected as a typical example of interstellar PAH molecules based on the following consideration: (1) 9-hydroxyfluorene has a relatively large size among the organic molecules contained with oxygenated functional groups; (2) 9-hydroxyfluorene is suitable for heating in the oven that can efficiently sublimates into the gas phase.

2 EXPERIMENTAL RESULTS

The experiments were performed on an experimental apparatus equipped with a quadrupole ion trap and reflection time-of-flight (QIT-TOF) mass spectrometer (details provided in Appendix A, Zhen et al. 2019a,b). C_{60}^+ was generated by electron impact ionization and filled into the trap within the time range of 0.0–4.0 s. Then a 355 nm laser (~ 20 mJ/pulse, 10 Hz, irradiation time amounting to 1.8 s, from 4.0–5.8 s) was used to irradiate the trapped C_{60}^+ to generate smaller fullerene cations. Under laser irradiation, the trapped fullerene cations underwent photo-fragmentation processes, i.e., they successively lost C_2 units to form a series of smaller fullerene cations (C_n^+ , $n=32, 34, \dots, 58$, Lifshitz 2000; Zhen et al. 2014). These newly formed fullerene cations subsequently reacted with gas-phase neutral 9-hydroxyfluorene molecules to form fullerene/9-hydroxyfluorene cluster cations (5.8–9.88 s), and then detected by the reflection time-of-flight mass spectrometer. All the species are observed as peaks with different mass/charge (m/z) in the mass spectrum, and can be identified given the initial reactants.

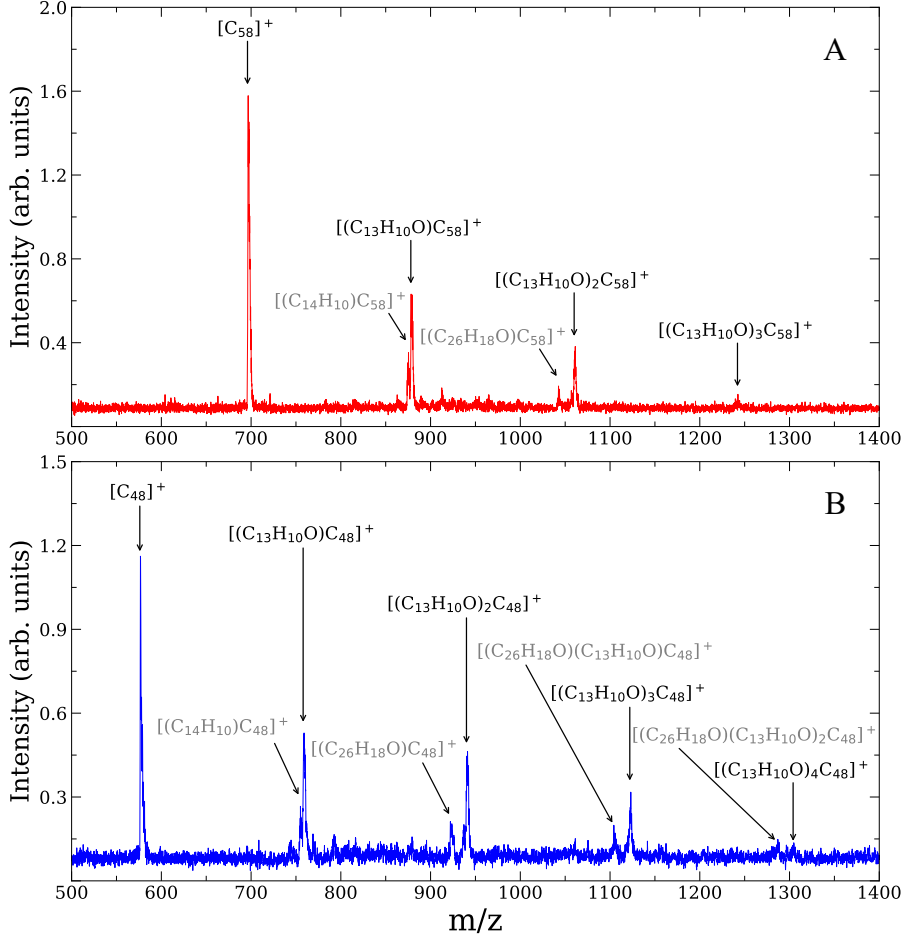


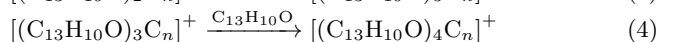
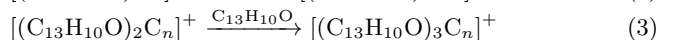
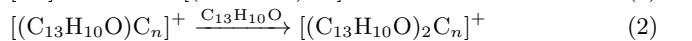
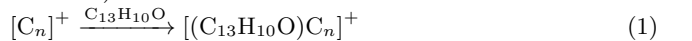
Figure 2. The resulting mass spectra of C_{58}^+ /9-hydroxyfluorene cluster cations (panel A), and C_{48}^+ /9-hydroxyfluorene cluster cations (panel B) when using the SWIFT technique. The cluster cation series are labeled (black), together with the fullerene/dimer clusters and contamination of fullerene/anthracene cluster cations (gray).

Fig. 1 presents the resulting mass spectrum of fullerene/9-hydroxyfluorene cluster cations, showing that a series of cationic clusters have been generated. Fullerene cations (C_n^+ , $n=36, 38, \dots, 60$; marked in red), and four groups of fullerene/9-hydroxyfluorene cluster cations are presented and labeled: mono- $C_{13}H_{10}O$ adducts ($[(C_{13}H_{10}O)C_n]^+$, $n=32, 34, \dots, 60$; marked in blue), di- $C_{13}H_{10}O$ adducts ($[(C_{13}H_{10}O)_2C_n]^+$, $n=32, 34, \dots, 58$; marked in green), tri- $C_{13}H_{10}O$ adducts ($[(C_{13}H_{10}O)_3C_n]^+$, $n=42, 44, \dots, 50$; marked in magenta), and tetra- $C_{13}H_{10}O$ adducts ($[(C_{13}H_{10}O)_4C_n]^+$, $n=44, 46, 48$; marked in cyan). Some mass peaks of species with similar m/z range may overlap. We also observed and labeled some additional mass peaks, which were formed as a side-product due to contaminations of anthracene ($C_{14}H_{10}$) in the ion trap chamber (Zhen et al. 2019b). For example, one series of additional peaks can be assigned as $[(C_{14}H_{10})C_n]^+$ ($n=48, 50, \dots, 60$; marked in purple).

Based on the observed new species, we supposed that fullerene/9-hydroxyfluorene cluster cations are formed through collision reactions between fullerene cations (C_n^+ , $n=32, 34, \dots, 60$) and neutral $C_{13}H_{10}O$ molecules, similarly to previous work on fullerene-PAH cationic clusters (Böhme 2016; Zhen et al. 2019b). The reaction process of fullerene

cations and $C_{13}H_{10}O$ was carried out through sequential steps, in which $C_{13}H_{10}O$ molecules were added repeatedly to the surface of fullerene cation cages (García-Hernández et al. 2013; Sato et al. 2013; Zhen et al. 2019a). As a result, a series of large fullerene/9-hydroxyfluorene cluster cations were formed. We note that only one $C_{13}H_{10}O$ molecule can be added to C_{60}^+ , while with the size of fullerene species decreased, more $C_{13}H_{10}O$ molecules can be added to smaller fullerene cations, suggesting an enhanced chemical reactivity for smaller fullerene cations.

The corresponding formation pathways for fullerene/9-hydroxyfluorene cluster cations are summarized below (equations 1-4):

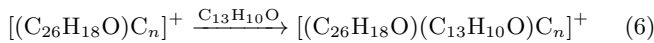
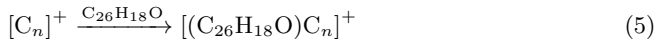


Due to the weak intensity and overlap with each other, some mass peaks cannot be identified in Fig. 1. To clarify that, we performed another experiment adopting the stored waveform inverse Fourier transform excitation (SWIFT) isolation technique (Doroshenko & Cotter 1996). In this experiment, when the laser irradiation ended, a SWIFT pulse

was applied to the end caps of the ion trap, allowing for the selection of the desired fullerene cations with a specific mass/charge (m/z) range to understand their reactions.

Fig. 2 displays two typical mass spectra for the clusters formed through reactions between individual fullerene cations (here, C_{58}^+ and C_{48}^+) and 9-hydroxyfluorene molecules, where the newly formed clusters for C_{58}^+ and C_{48}^+ were observed and labeled in Fig. 2(A) and Fig. 2(B), respectively. The observed mass peaks for fullerene cations (C_{58}^+/C_{48}^+), fullerene/9-hydroxyfluorene clusters ($[(C_{13}H_{10}O)_{1-3}C_{58}]^+$ and $[(C_{13}H_{10}O)_{1-4}C_{48}]^+$) are identified, together with fullerene/anthracene cluster cations ($[(C_{14}H_{10})C_{58}]^+$ and $[(C_{14}H_{10})C_{48}]^+$) resulting from contamination. The mass spectra when using the SWIFT technique for the two individual fullerene cations show a similar reaction process, implying the sequential steps for the reactions of fullerene cations with $C_{13}H_{10}O$ molecules.

Interestingly, we also observed several additional peaks in Fig. 2. These additional peaks are formed as side-products due to the neutral dimer 9-hydroxyfluorene molecule ($C_{26}H_{18}O$, $m/z=346$) that formed in the heat processes through dehydration pathways. For example, as shown in Fig. 2(B), three additional peaks can be assigned as: $[(C_{26}H_{18}O)C_{48}]^+$ ($m/z=922$), $[(C_{26}H_{18}O)(C_{13}H_{10}O)C_{48}]^+$ ($m/z=1104$), and $[(C_{26}H_{18}O)(C_{13}H_{10}O)_2C_{48}]^+$ ($m/z=1286$). The corresponding formation pathways for the fullerene/dimer cluster cations are summarized below (equations 5-6):



3 THEORETICAL CALCULATION RESULTS

To understand the formation mechanism of the fullerene/9-hydroxyfluorene cluster cation system, the reaction channels occurring on the fullerene surface during the accretion processes were theoretically studied. Here, the structures of fullerene (C_{60}) cation and a defective fullerene (C_{58}) cation along with $C_{13}H_{10}O$ and its dimer formed by dehydration reactions ($C_{26}H_{18}O$), and the reaction pathways of $C_{60}^+ + C_{13}H_{10}O$ and $C_{58}^+ + C_{13}H_{10}O/C_{26}H_{18}O$ were performed through quantum theoretical calculations.

All the calculations were performed by the Gaussian 16 program (Frisch et al. 2016) package, using density functional theory employing the hybrid functional B3LYP (Becke 1992; Lee et al. 1988) with the 6-311++G(d,p) basis set, which is consistent with previous study (e.g., Hu et al. 2023). We followed the minimum energy pathway of the Van der Waals cluster or the covalently bonded cluster and, at each step, calculated the molecular geometries and binding energies. The negative and positive binding energies correspond to exothermic and endothermic reactions. Since we use the helium atoms as a stabilization (Zhen et al. 2019a,b), the molecular collision in our laboratory is at a low velocity. Thus, we think the exothermic reactions are dominant and easier to occur, while the endothermic reactions could not occur. To account for the intermolecular interactions, dispersion correction (D3, Grimme et al. 2011) was considered for each system. The vibrational frequencies were calculated for the optimized geometries to verify that these geometries correspond

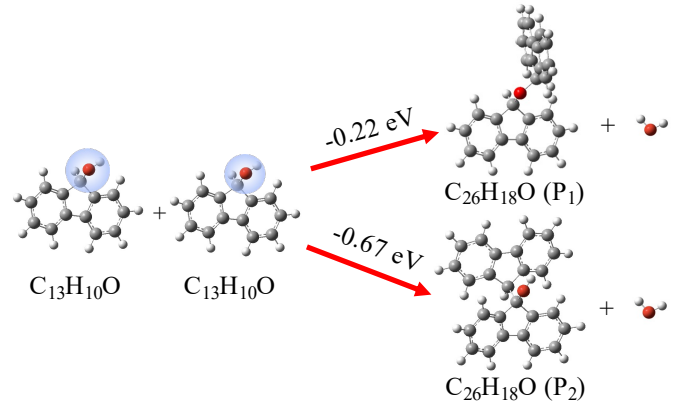


Figure 3. The formation pathways and optimized geometries of $C_{26}H_{18}O$. The negative energy is corresponding to the exothermic reaction.

to the minima on the potential energy surface. Furthermore, the zero-point vibrational energy was obtained from the frequency calculation to correct the molecular energy.

For fullerene cations (C_{60}^+ and C_{58}^+), the molecular structures were mainly consistent with that in our previous work (Zhen et al. 2019a,b; Hu et al. 2021a, 2023). In this work, we assumed that there was only the C_2 loss at a local position and no carbon skeleton rearrangement during the electron impact ionization and fragmentation (Zhen et al. 2019b; Candian et al. 2019). Fullerene cations (C_{60}^+ and C_{58}^+) and their derivate cationic clusters have an odd number of electrons, resulting in an open-shell doublet ground state (spin multiplicity of 2) for the ground electronic state. The neutral $C_{13}H_{10}O$ and $C_{26}H_{18}O$ have closed-shell electronic structures, and their spin multiplicity is 1.

The calculated results for the formation pathways and optimized geometries of $C_{26}H_{18}O$ are shown in Fig. 3. The calculation results for $C_{60}^+ + C_{13}H_{10}O$ are shown in Fig. 4. The calculation results for C_{58}^+ with $C_{13}H_{10}O$ are provided in Fig. 5-8. The calculation results for $C_{58}^+ + C_{26}H_{18}O$ are provided in Fig. 9.

3.1 The formation pathways and optimized geometries of $C_{26}H_{18}O$

The formation pathways and optimized geometries of $C_{26}H_{18}O$ are illustrated in Fig. 3. $C_{26}H_{18}O$ is mainly formed through an intermolecular dehydration pathway during heating in the oven. To form $C_{26}H_{18}O$ (P₁), an ether (C-O-C) bond is newly formed with exothermic energy of -0.22 eV (-5.0 kcal mol⁻¹); for the formation of $C_{26}H_{18}O$ (P₂), a C-C single bond is newly formed with exothermic energy of -0.67 eV (-15.5 kcal mol⁻¹). Based on the calculation results, both molecules $C_{26}H_{18}O$ (P₁ & P₂) are selected as the dehydration products of $C_{13}H_{10}O$ for the further calculations of the cluster formation.

3.2 Calculated results of $C_{60}^+ + C_{13}H_{10}O$

Fig. 4 depicts the formation channel of the adduct between C_{60}^+ and $C_{13}H_{10}O$. Fig. 4(A) is for the formation of the Van der Waals clusters, and Fig. 4(B & C) for the formation of the covalently bonded clusters, consistent with previous works (e.g. Zhen et al. 2019b; Hu et al. 2021b, 2023)

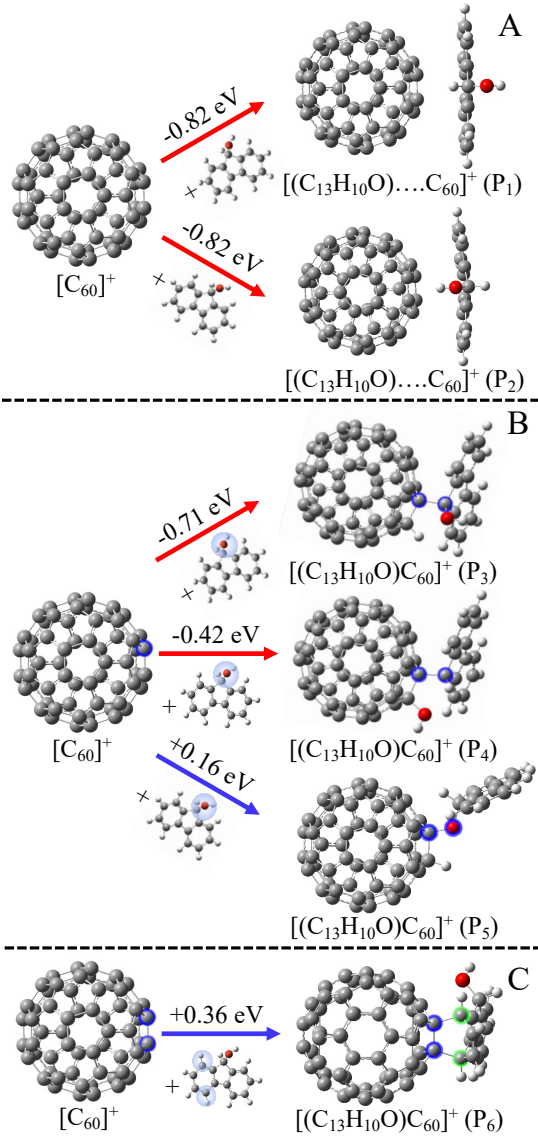


Figure 4. The reaction pathways of $C_{60}^+ + C_{13}H_{10}O$. The negative and positive binding energies correspond to exothermic and endothermic reactions.

As shown in Fig. 4(A), the Van der Waals cluster molecules, $[(C_{13}H_{10}O)\dots C_{60}]^+$ (P₁) and $[(C_{13}H_{10}O)\dots C_{60}]^+$ (P₂) are formed in two different molecular alignments. The reactions are exothermic by the same energy of -0.82 eV (-18.9 kcal mol⁻¹). Therefore, the molecular alignments, e.g., H-C-OH or HO-C-H, do not affect the formation of the Van der Waals cluster molecules. Furthermore, in order to better demonstrate the binding characteristics of these newly formed molecular clusters, the three-dimensional (3D) images of the Mulliken charge separation, highest occupied molecular orbital (HOMO) and lowest unoccupied molecular orbital (LUMO) of these molecules are obtained and provided in the Appendix B (Fig. B1), respectively.

In Fig. 4(B), three possible reaction pathways concerning the functional groups, -CHOH unit, of $C_{13}H_{10}O$ are obtained. For the formation of $[(C_{13}H_{10}O)C_{60}]^+$ (P₃), C_{60}^+ and $C_{13}H_{10}O$ are connected by a newly formed C-C single bond, in which one C atom is from C_{60}^+ and the other from -CHOH group. Meanwhile, the H atom from the CH unit in

the -CHOH group directly migrates to the nearby carbon on the surface of C_{60}^+ , forming a new C-H bond. The reaction has an exothermic reaction energy of -0.71 eV (-16.4 kcal mol⁻¹). To form $[(C_{13}H_{10}O)C_{60}]^+$ (P₄), C_{60}^+ and $C_{13}H_{10}O$ are connected by a newly formed C-C single bond, in which one C atom is from C_{60}^+ and the other from -CHOH group. Meanwhile, the OH unit in the -CHOH group directly migrates to the nearby carbon on the surface of C_{60}^+ , forming a new C-OH bond. The reaction is exothermic by -0.42 eV (-9.7 kcal mol⁻¹). To form $[(C_{13}H_{10}O)C_{60}]^+$ (P₅), C_{60}^+ and $C_{13}H_{10}O$ are connected by a newly formed C-O single bond, in which the C atom is from C_{60}^+ and the O atom from -CHOH group. Meanwhile, the H atom from the OH group in the -CHOH group directly migrates to the nearby carbon on the surface of C_{60}^+ , forming a new C-H bond. The reaction is endothermic by $+0.16$ eV ($+3.7$ kcal mol⁻¹). Thus, we suppose this reaction pathway cannot occur in the ISM.

Moreover, concerning the aromatic ring of $C_{13}H_{10}O$, the possible reaction pathway of $[(C_{13}H_{10}O)C_{60}]^+$ (P₆) is illustrated in Fig. 4(C), in which C_{60}^+ and $C_{13}H_{10}O$ are connected by double C-C bridge bonds, similar to previous works (Petrie & Bohme 1993; Sato et al. 2013; Zhen et al. 2019b). The reaction is endothermic by $+0.36$ eV ($+8.3$ kcal mol⁻¹), and we suppose it is unlikely to occur.

The exothermic energy for the formation of $[(C_{13}H_{10}O)C_{60}]^+$ (P₁-P₄), with binding energies between -0.42 and -0.82 eV (-9.7 and -18.9 kcal mol⁻¹), is relatively higher and can stabilize the whole clusters. Thus, we propose that $[(C_{13}H_{10}O)C_{60}]^+$ formed in the laboratory is a mixed cluster with different possible isomers.

3.3 Calculated results of $C_{58}^+ + C_{13}H_{10}O$

For the interaction of C_{58}^+ with $C_{13}H_{10}O$, due to the structure of C_{58}^+ (e.g., Lee & Han 2004), as shown in Fig. 6, there are two types of reaction pathways needed to be considered: $C_{13}H_{10}O$ “landing” on the 6 C-ring, and $C_{13}H_{10}O$ “landing” on the 7 C-ring, which is in agreement with previous works (Zhen et al. 2019b; Hu et al. 2023). The calculation results are presented in Fig. 5-7, respectively.

3.3.1 Calculated results of C_{58}^+ (6 C-ring) + $C_{13}H_{10}O$

For the reaction type of $C_{13}H_{10}O$ “landing” on the 6 C-ring of C_{58}^+ , similar to the reaction of $C_{60}^+ + C_{13}H_{10}O$, the formation channel of $[(6-C_{13}H_{10}O)C_{58}]^+$ is demonstrated in Fig. 5.

In Fig. 5(A), the Van der Waals cluster molecules, $[(6-C_{13}H_{10}O)\dots C_{58}]^+$ (P₁) is formed in a typical molecular alignment, and the reaction is exothermic by -0.76 eV (-17.5 kcal mol⁻¹). Three possible reaction pathways concerning the -CHOH unit of $C_{13}H_{10}O$ are obtained in Fig. 5(B). $[(6-C_{13}H_{10}O)C_{58}]^+$ (P₂) is formed by the H transfer reaction with exothermic energy of -0.36 eV (-8.3 kcal mol⁻¹), in which C_{58}^+ and $C_{13}H_{10}O$ are connected by a newly formed C-C single bond with H from CH group migrating to the nearby carbon on the surface of C_{58}^+ and forming a new C-H bond. To form $[(6-C_{13}H_{10}O)C_{58}]^+$ (P₃), C_{58}^+ and $C_{13}H_{10}O$ are connected by a newly formed C-C single bond with OH migrating to the nearby carbon on the surface of C_{58}^+ and forming a new C-OH bond. The reaction is exothermic by

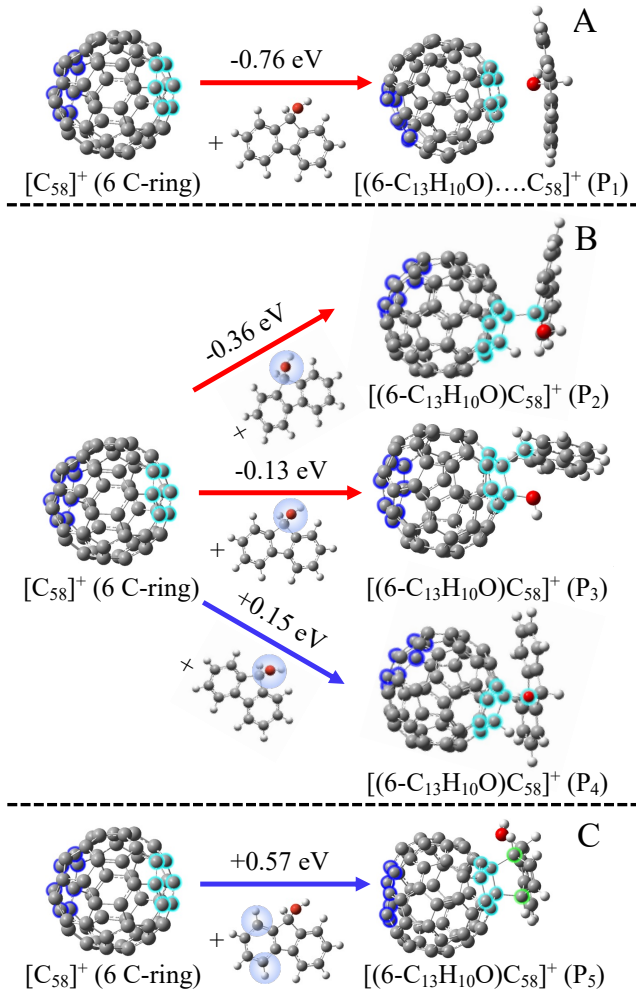


Figure 5. The reaction pathways of C_{58}^+ (6 C-ring) + $C_{13}H_{10}O$. The negative and positive binding energies correspond to exothermic and endothermic reactions. The 7 C-ring and 6 C-ring are highlighted.

-0.13 eV (-3.0 kcal mol $^{-1}$). $[(6-C_{13}H_{10}O)C_{58}]^+$ (P₄) is also formed by the H transfer reaction, in which the H atom is from the OH group. The reaction has an endothermic energy of $+0.15$ eV ($+3.5$ kcal mol $^{-1}$) and cannot occur. Moreover, $[(6-C_{13}H_{10}O)C_{58}]^+$ (P₅) illustrated in Fig. 5(C) is the product concerning the aromatic ring of $C_{13}H_{10}O$, in which C_{58}^+ and $C_{13}H_{10}O$ are connected by double C-C bonds. The reaction is endothermic by $+0.57$ eV ($+13.1$ kcal mol $^{-1}$) and cannot occur.

By comparing the formation of $[(6-C_{13}H_{10}O)C_{58}]^+$ with that of $[(C_{13}H_{10}O)C_{60}]^+$, we find no variation of the binding energy with the same reaction modes, implying no deformation for the 6 C-ring of C_{58}^+ .

3.3.2 Calculated results of C_{58}^+ (7 C-ring) + $C_{13}H_{10}O$ (I)

Due to the multi-carbon reaction sites of C_{58}^+ (7 C-ring) that can be applied for the further adduct reactions, we carried out the chemical reactivity for these multi-carbon reaction sites of C_{58}^+ (7 C-ring) with $C_{13}H_{10}O$. Three factors are considered for the chemical reactivity, including the reaction mode with $C_{13}H_{10}O$, the combining carbon reaction site, and

the reaction boundary. The obtained reaction pathways and optimized geometries of products are shown in Fig. 6.

One typical reaction mode is selected: the OH group transfer reactions. Thus, these seven carbon combining reaction sites of C_{58}^+ (7 C-ring) can be divided and labeled as 1, 2 and 2', 3 and 3', 4 and 4'. Since the OH group transfer reaction pathways need two adjacent carbon sites along the boundary of the 7 C-ring, four combination modes can be obtained as (1,2)=(1,2'), (2,3)=(2',3'), (3,4)=(3',4'), (4,4'). (1,2)=(1,2') and (4,4') are the boundaries of the 7 C-ring and 6 C-ring, while (2,3)=(2',3') and (3,4)=(3',4') are the boundaries of the 7 C-ring and 5 C-ring.

As demonstrated in Fig. 6, the combination modes of (2,3) and (3,4) have a higher reactivity than (1,2) and (4,4'). The formation reaction pathways of $[(7-C_{13}H_{10}O)C_{58}]^+$ ($2C-C$, $3C-OH$ & $3C-C$, $2C-OH$) or $[(7-C_{13}H_{10}O)C_{58}]^+$ ($3C-C$, $4C-OH$ & $4C-C$, $3C-OH$) are exothermic by -0.82 and -0.63 eV (-18.9 and -14.5 kcal mol $^{-1}$), or -0.75 and -0.65 eV (-17.3 and -15.0 kcal mol $^{-1}$), respectively. However, the formation reaction pathways of $[(7-C_{13}H_{10}O)C_{58}]^+$ ($4C-C$, $4'C-OH$) or $[(7-C_{13}H_{10}O)C_{58}]^+$ ($2C-C$, $1C-OH$ & $1C-C$, $2C-OH$) are endothermic $+0.31$ eV ($+7.2$ kcal mol $^{-1}$) or $+0.48$ and $+0.50$ eV ($+11.1$ and $+11.5$ kcal mol $^{-1}$), respectively, and unlikely to occur.

Accordingly, the reaction tends to occur along the boundary of the 7 C-ring and 5 C-ring rather than the boundary of the 7 C-ring and 6 C-ring, suggesting that the combination mode of (2,3)=(3,4) has a higher chemical reactivity, which is in agreement with [Petrie & Bohme \(1993\)](#). Therefore, we choose the combination mode of (2,3) for further calculations of the cluster formation.

3.3.3 Calculated results of C_{58}^+ (7 C-ring) + $C_{13}H_{10}O$ (II)

Based on the calculated results, the reaction pathways of C_{58}^+ (7 C-ring) with (2,3) + $C_{13}H_{10}O$ for different reaction modes are obtained and illustrated in Fig. 7.

In Fig. 7(A), the Van der Waals cluster molecule, $[(7-C_{13}H_{10}O)...C_{58}]^+$ (P₁) is formed in one typical molecular alignment, and the reaction is exothermic by -0.92 eV (-21.2 kcal mol $^{-1}$). In Fig. 7(B), three possible reaction pathways concerning the -CHOH unit of $C_{13}H_{10}O$ are obtained. To form $[(7-C_{13}H_{10}O)C_{58}]^+$ (P₂), C_{58}^+ and $C_{13}H_{10}O$ are connected by a newly formed C-C single bond with the transfer of H from CH group to the adjacent carbon on the 7 C-ring surfaces of C_{58}^+ and the formation of a C-H single bond. The reaction has an exothermic energy of -1.12 eV (-25.8 kcal mol $^{-1}$). The formation pathways of $[(7-C_{13}H_{10}O)C_{58}]^+$ (P₃ & P₄), with the transfer of OH unit and H atom from OH group, have an exothermic reaction energy of -0.82 and -0.80 eV (-18.9 and -18.4 kcal mol $^{-1}$), respectively. Moreover, $[(7-C_{13}H_{10}O)C_{58}]^+$ (P₅) illustrated in Fig. 7(C) is the product concerning the aromatic ring of $C_{13}H_{10}O$, in which C_{58}^+ and $C_{13}H_{10}O$ are connected by double C-C bonds. The reaction is endothermic by $+0.25$ eV ($+5.8$ kcal mol $^{-1}$) and cannot occur.

The exothermic energy of $[(7-C_{13}H_{10}O)C_{58}]^+$ is much higher than that of $[(C_{13}H_{10}O)C_{60}]^+$ or $[(6-C_{13}H_{10}O)C_{58}]^+$ with the same reaction modes, suggesting that there is an enhanced chemical reactivity of the 7 C-ring in C_{58}^+ , consisting well with previous works (e.g. [Zhen et al. 2019b](#); [Hu et al. 2021b](#)). Both the Van der Waals clusters, $[(7-$

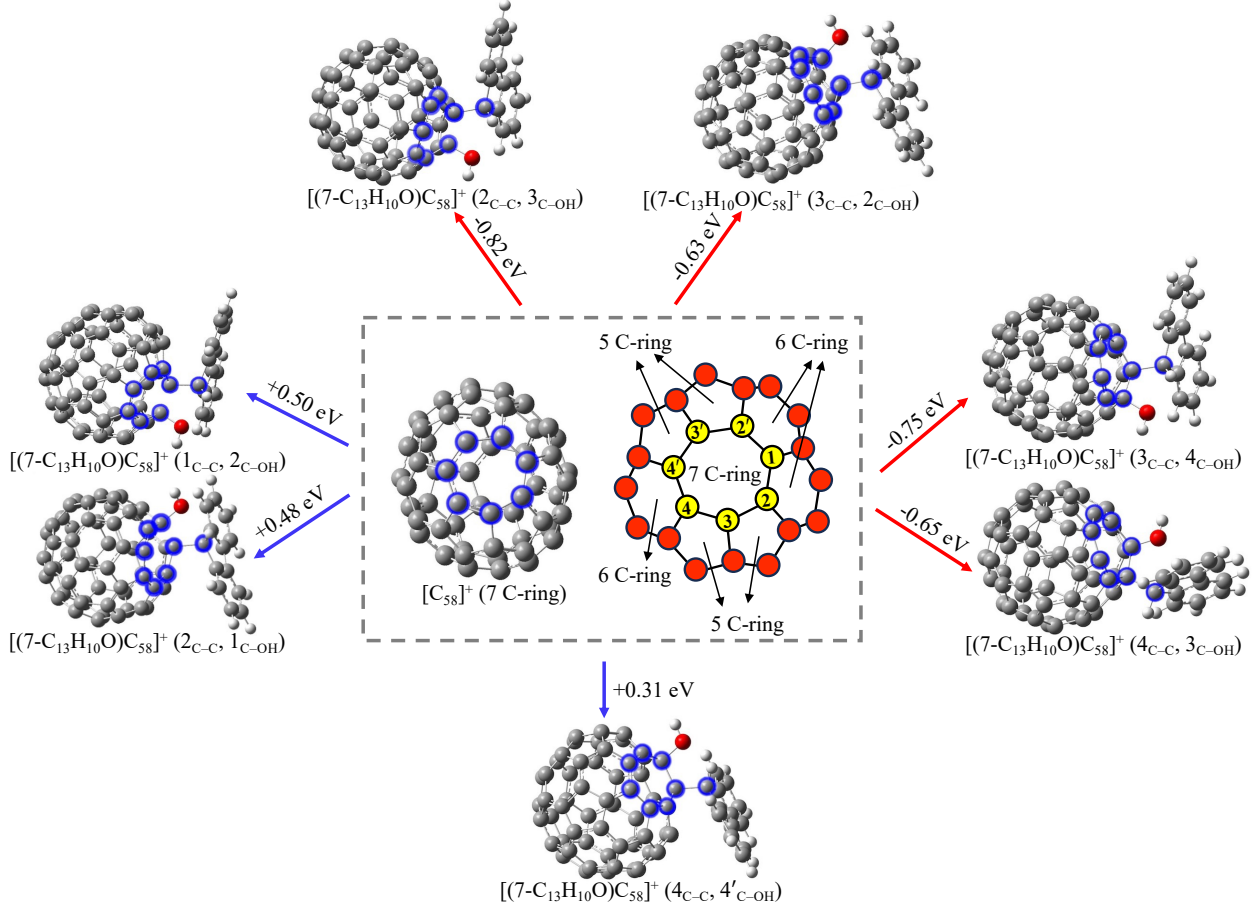


Figure 6. The OH transfer reactions between C_{58}^+ (7 C-ring) and $C_{13}H_{10}O$ with different combination sites. The negative and positive binding energies correspond to exothermic and endothermic reactions. The 7 C-ring is highlighted.

$C_{13}H_{10}O$)... C_{58}^+ (P₁) and the covalently bonded clusters, $[(7-C_{13}H_{10}O)C_{58}]^+$ (P₂-P₄) have relatively high exothermic energy and may exist.

Combining the calculation results for $[(6-C_{13}H_{10}O)C_{58}]^+$, we propose that $[(C_{13}H_{10}O)C_{58}]^+$ formed in the laboratory is also a mixed cluster with different possible isomers. Moreover, C_{58}^+ has a higher chemical reactivity than C_{60}^+ , which is mainly attributed to the newly formed deformed 7 C-ring.

3.4 Calculated results of $[(C_{13}H_{10}O)C_{58}]^+ + C_{13}H_{10}O$

The formation routes for larger fullerene/9-hydroxyfluorene cluster cations were also investigated to elucidate the formation mechanism for larger C_{58}^+ /9-hydroxyfluorene clusters. Fig. 8 displays the reaction routes for the formation of di- $C_{13}H_{10}O$ adducts, $(C_{13}H_{10}O)_2C_{58}^+$, with considered three isomers of $(C_{13}H_{10}O)C_{58}^+$.

Due to the spatial effect, we suppose that the second $C_{13}H_{10}O$ will be added on the 6 C-ring surfaces opposite to the 7 C-ring of $[(7-C_{13}H_{10}O)C_{58}]^+$ through the Van der Waals bond. $[(7-C_{13}H_{10}O)(6-C_{13}H_{10}O)....C_{58}]^+$ (P₁) and $[(7-C_{13}H_{10}O)....C_{58}....(6-C_{13}H_{10}O)]^+$ (P₂) are the products formed by the reaction pathways described above. The reactions are exothermic by -0.71 and -0.70 eV (-16.4 and -16.1 kcal mol⁻¹), respectively. We note that on the 6 C-ring surfaces, there is no variation in binding energies formed by C_{58}^+ or $[(7-C_{13}H_{10}O)C_{58}]^+$ with $C_{13}H_{10}O$.

Similarly, we obtained the reaction pathways

from $[(6-C_{13}H_{10}O)....C_{58}]^+$ (P₁) to $[(7-C_{13}H_{10}O)(6-C_{13}H_{10}O)....C_{58}]^+$ (P₁) and $[(7-C_{13}H_{10}O)....C_{58}....(6-C_{13}H_{10}O)]^+$ (P₂), with high exothermic energy of -1.07 and -0.86 eV (-24.7 and -19.8 kcal mol⁻¹), respectively, suggesting the diversity of the reaction pathways for the formation of larger fullerene/9-hydroxyfluorene cluster cations.

The exothermic energy for the formation of $[(C_{13}H_{10}O)_2C_{58}]^+$ is higher, without a difference when compared with the formation of $[(C_{13}H_{10}O)C_{58}]^+$. Thus, consistent with the experimental results, $(C_{13}H_{10}O)_2C_{58}^+$ can easily formed in the laboratory and is a mixed cluster with different possible isomers.

3.5 Calculated results of C_{58}^+ (7 C-ring) + $C_{26}H_{18}O$

Due to the high chemical reactivity shown in Fig. 6, we selected C_{58}^+ (7 C-ring) with (2,3) for the formation of $[(C_{26}H_{18}O)C_{58}]^+$. The reaction pathways of C_{58}^+ (7 C-ring) + $C_{26}H_{18}O$ are illustrated in Fig. 9, and we only provide reaction pathways related to the oxygenated functional groups (e.g., hydroxyl, OH and ether, C-O-C).

Fig. 9(A) shows the reaction pathways related to the C-O-C group in $C_{26}H_{18}O$ (P₁). $[(7-C_{26}H_{18}O)C_{58}]^+$ (a-P₁) is formed by H atom transfer reaction with exothermic energy of -1.40 eV (-32.3 kcal mol⁻¹), in which the C atom from the C-O-C group is added to the 7 C-ring of C_{58}^+ with the formation of a C-C single bond, and the H atom connected to the C-O-C

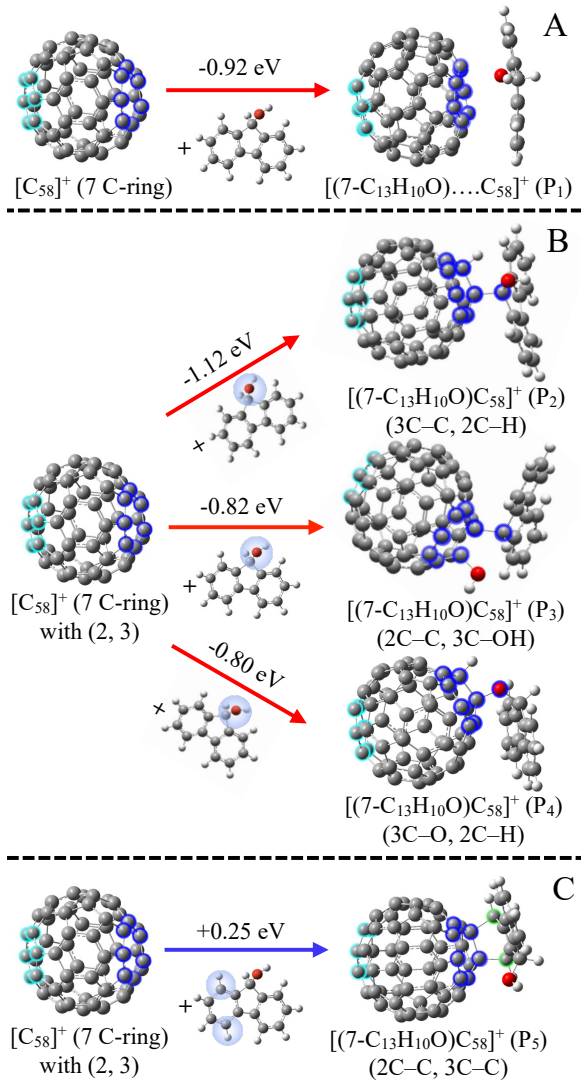


Figure 7. The reaction pathways of C_{58}^+ (7 C-ring) with (2,3) + $C_{13}H_{10}O$. The negative and positive binding energies correspond to exothermic and endothermic reactions. The 7 C-ring and 6 C-ring are highlighted.

group migrates to the adjacent carbon. $[(7-C_{26}H_{18}O)C_{58}]^+$ (a-P₂) is formed with the fracture of the C-O-C group. Releasing energy of -1.17 eV (-27.0 kcal mol⁻¹), two fragments after the fracture of the C-O-C group are connected to nearby carbon atoms on 7 C-ring of C_{58}^+ .

The reaction pathways related to the OH group in $C_{26}H_{18}O$ (P₂) are selected and calculated in Fig. 9(B). Since the exothermic energy of the OH group transfer reaction is close to that of the H atom transfer reaction on C_{58}^+ (7 C-ring), we only show two examples of H atom transfer reaction pathways. Accordingly, $(7-C_{26}H_{18}O)C_{58}^+$ (b-P₁) is formed with the fracture of C-H bond near the OH group releasing energy of -1.07 eV (-24.7 kcal mol⁻¹), and $[(7-C_{26}H_{18}O)C_{58}]^+$ (b-P₂) is formed with the fracture of O-H bond releasing energy of -0.59 eV (-13.6 kcal mol⁻¹).

The exothermic energy for the formation of $[(7-C_{26}H_{18}O)C_{58}]^+$ is higher and can stabilize the whole clusters. Thus, we propose that $[(C_{26}H_{18}O)C_{58}]^+$ formed in the laboratory is a mixed cluster with different possible isomers. Interestingly, $C_{26}H_{18}O$ is a large functionalized PAH molecule

(with 45 atoms, and ~ 2 nm in size) that can still react easily with fullerene species in the gas phase, which can prove again that fullerene species readily react with large molecules.

4 DISCUSSION

During the collision reactions between fullerene cations and 9-hydroxyfluorene molecules, $C_{13}H_{10}O$ and $C_{26}H_{18}O$ are added to the surface of fullerene through sequential steps, resulting in a variety of fullerene/9-hydroxyfluorene cluster cations (García-Hernández et al. 2013; Sato et al. 2013; Böhme 2016; Zhen et al. 2019a,b). According to our calculations, the bonding ability, i.e., the reaction surfaces, reaction modes, and combination sites, play a decisive role in the cluster formation processes.

To the reaction surfaces: two different reaction surfaces are considered— $C_{13}H_{10}O$ “landing” on the 6 C-ring and $C_{13}H_{10}O$ “landing” on the 7 C-ring, which is in agreement with previous works (Zhen et al. 2019b; Hu et al. 2023). For 6 C-ring (both in C_{60}^+ and C_{58}^+), the stable product is the Van der Waals complex (with exothermic energy of ~ 0.8 eV, 18.4 kcal mol⁻¹); for 7 C-ring, 9-hydroxyfluorene tends to form covalently bonded clusters and connect directly to the 7 C-ring surfaces of C_{58}^+ (with exothermic energy of ~ 1.1 eV, 25.4 kcal mol⁻¹). The exothermic energy of the covalently bonded cluster formed on the 7 C-ring surfaces is higher than that on the 6 C-ring surfaces. Therefore, the enhanced chemical reactivity for smaller fullerene cations is mainly attributed to the deformed rings (e.g., 7 C-ring in C_{58}^+) (e.g. Zhen et al. 2019b; Hu et al. 2021b, 2023).

To the reaction modes: five different reaction modes are taken into consideration—the Van der Waals interaction (e.g. Zhen et al. 2019b; Hu et al. 2023), the H transfer reaction from CH unit, the H transfer reaction from OH group, the OH group transfer reaction, and the reaction concerning the aromatic ring with the newly formed double C-C bonds (Petrie & Bohme 1993; Sato et al. 2013; Böhme 2016; Zhen et al. 2019b). We can see that the reaction concerning the aromatic ring is endothermic, i.e., fullerenes and 9-hydroxy fluorene molecules are difficult to form the cluster connected by double C-C bonds (Zhen et al. 2019a,b).

To the combination sites: due to the geometric structure of 7 C-ring, four combination modes are considered for the OH group transfer reactions, (1,2)=(1,2'), (2,3)=(2',3'), (3,4)=(3',4'), (4,4'). By comparing the binding energies for different combination modes, the chemical reactivity can be obtained as follows: (2,3)=(2',3') \sim (3,4)=(3',4') $>$ (4,4') $>$ (1,2)=(1,2'). Thus, we can conclude that the formation of C_{58}^+ /9-hydroxyfluorene cluster tends to occur along the boundary of the 7 C-ring and 5 C-ring rather than the boundary of the 7 C-ring and 6 C-ring, which suggests that the combination sites adjacent to 5 C-rings may have a higher chemical reactivity (Petrie & Bohme 1993).

Overall, we infer that during the formation of fullerene/9-hydroxyfluorene cluster cations, the first $C_{13}H_{10}O$ molecule may initially be connected to the deformed cage surfaces of smaller fullerene cations. After the deformed rings are occupied, other $C_{13}H_{10}O$ molecules will be added to the 6 C-ring surfaces by Van der Waals bonds. As the number of C atoms decreases, there may be more deformed rings

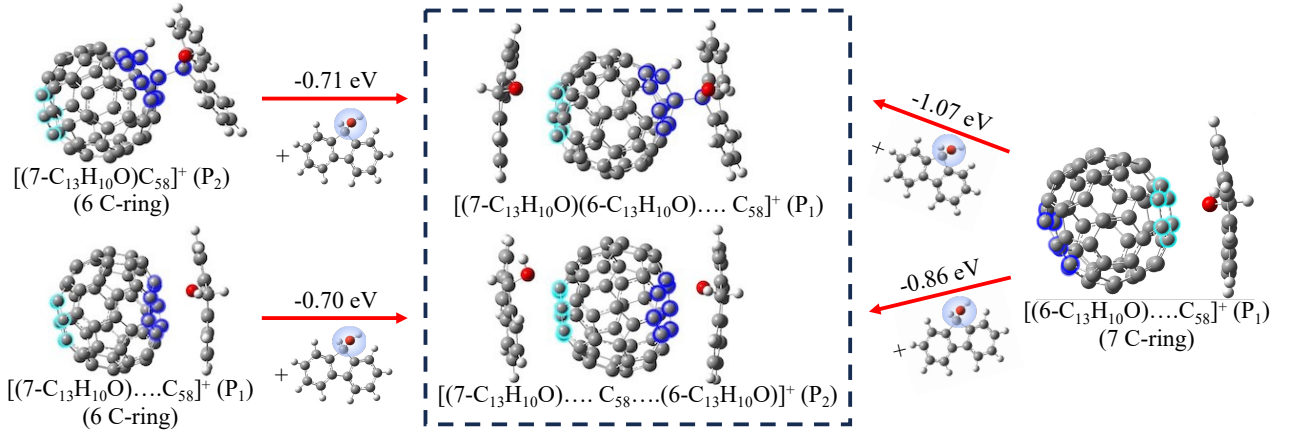


Figure 8. The reaction pathways of di- $C_{13}H_{10}O$ adducts, $(C_{13}H_{10}O)_2C_{58}^+$. Both $[(7-C_{13}H_{10}O)C_{58}]^+$ (6 C-ring) + $C_{13}H_{10}O$ and $[(6-C_{13}H_{10}O)C_{58}]^+$ (7 C-ring) + $C_{13}H_{10}O$ were taken into consideration. The negative binding energy corresponds to the exothermic reaction. The 7 C-ring and 6 C-ring are highlighted.

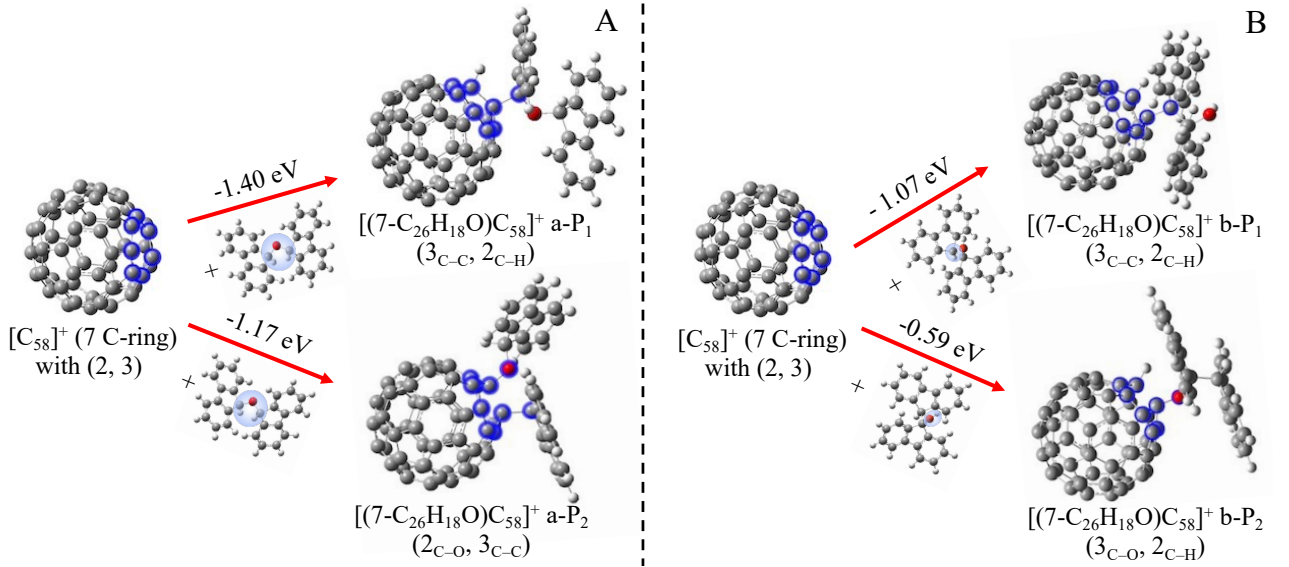


Figure 9. The Reaction pathways of C_{58}^+ (7 C-ring) with (2,3) + $C_{26}H_{18}O$. The negative binding energy corresponds to the exothermic reaction. The 7 C-ring is highlighted.

in smaller fullerene cations (e.g. Hu et al. 2021b). Therefore, more $C_{13}H_{10}O$ molecules can be added to the cage surfaces of smaller fullerene cations, resulting in various large fullerene/9-hydroxyfluorene cluster cations (Zhen et al. 2019a,b; Hu et al. 2021a).

5 ASTRONOMICAL IMPLICATIONS

In interstellar environment, the forms and states of fullerene molecules are affected and constrained by surrounding environmental factors, such as interstellar UV radiation, the flux of H atoms, hydrogen ions, and other coexisting molecules (García-Hernández et al. 2010, 2013; Dunk et al. 2013; Omont 2016). These environmental factors provide feedback and constraints on the states and forms of these fullerene molecules at their different evolution periods. Based on the interstellar co-evolution network, in this work, the fullerene molecules under the environmental factors of coexisting oxygenated functional

substituted PAH molecules are studied through experiments and theoretical quantum calculations.

The experimental results show that the reactions between fullerene cations (C_n^+ , $n=32, 34, \dots, 60$) and neutral 9-hydroxyfluorene molecules can occur in the gas phase. Fullerene/9-hydroxyfluorene cluster cations are formed through a sequential-step pathway, in which 9-hydroxyfluorene molecules are added repeatedly onto the cage surface of fullerene cations (García-Hernández et al. 2013; Sato et al. 2013; Zhen et al. 2019a). With the number of C atoms decreasing, more $C_{13}H_{10}O$ molecules can be added to smaller fullerene cations, suggesting an enhanced chemical reactivity for these smaller fullerene cations. The higher reactivity of small fullerenes may be attributed to the diversity of molecular structures (Petrie & Bohme 1993; Böhme 2016; Zhen et al. 2019b; Hu et al. 2021b) generated by UV laser photolysis, including caged, semi-caged, or planar structures (Berné & Tielens 2012; Candian et al. 2019). 9-hydroxyfluorene molecules have a relatively low chemical re-

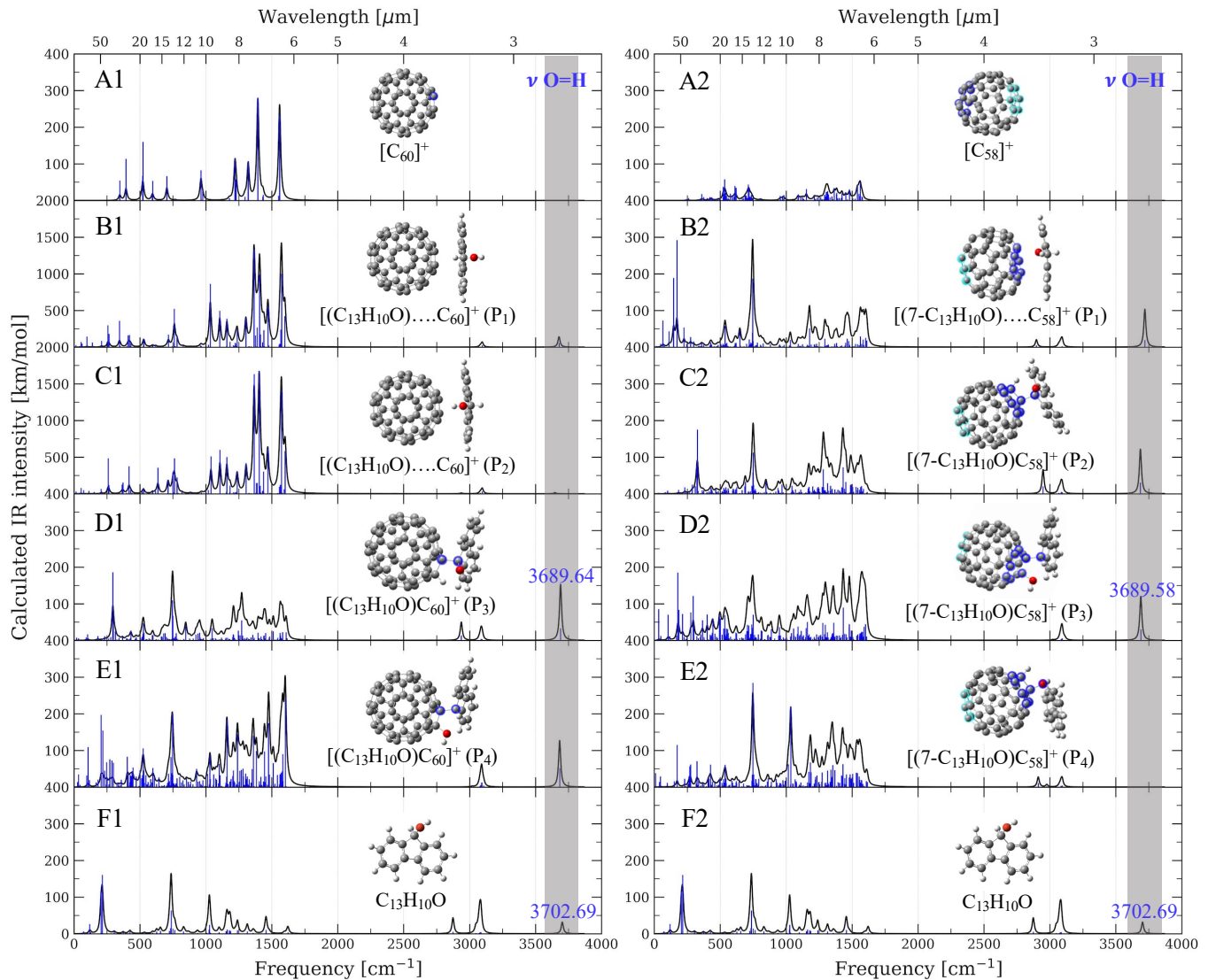


Figure 10. Computed IR spectra and vibrational normal modes for fullerene/9-hydroxyfluorene cluster cations: panels (A1–F1) are for $C_{60}^+ + C_{13}H_{10}O$, and panels (A2–F2) for $C_{58}^+ + C_{13}H_{10}O$, respectively. The vibrational band positions were scaled by 0.967 for C–H stretch mode and 0.980 for all other modes.

activity in the reaction with fullerene cations compared with other substituted derivative PAHs, such as anthracene, 9-methylanthracene, 9-vinylanthracene and 9-aminoanthracene (Zhen et al. 2019a,b; Hu et al. 2021a), indicating the effect of oxygenated functional group on the chemical reactivity.

From the results of the theoretical calculation, the molecular structure of fullerene/9-hydroxyfluorene cluster cations are diverse. The Van der Waals complexes are stable and may be readily formed when $C_{13}H_{10}O$ molecules are added to the 6 C-ring surfaces. In the reactions on the 7 C-ring surfaces, 9-hydroxyfluorene tends to be covalently bonded with fullerene cations. The higher exothermic energy for 7 C-ring surfaces also suggests an enhanced chemical reactivity of smaller fullerene cations (e.g. Zhen et al. 2019b; Hu et al. 2021b, 2023), which is well consistent with the experimental results. The relative chemical reactivity of these species is very important in the evolution network of the ion-molecular reaction, which affects the abundance ratio of formed species (Jäger et al. 2009; Montillaud et al. 2013; Zhen et al. 2019b).

Since the fullerenes (e.g., C_{60} and C_{60}^+) have been

confirmed in the ISM, we expect their derivatives (i.e., fullerene/PAH clusters) might also coexist in space. However, due to the non-overlapping spatial distributions of fullerenes and smaller PAHs in planetary nebulae, we do not propose fullerene/PAH adducts as contributors. Especially in the harsh interstellar environment, small PAHs and their derivatives hardly survived (Tielens 2008). Nevertheless, species formed by reactions between fullerene cations and molecules found in planetary nebulae may be involved (García-Hernández et al. 2010; Cami et al. 2010). The co-existing molecules, not only specific PAHs but also mixed PAHs containing oxygenated functional groups (OH or C–O–C), may be involved in the growth of dust particles.

In addition, we also obtained the dehydrated product $C_{26}H_{18}O$ in the heat processes, which is a large functionalized PAH molecule (with 45 atoms, and in ~ 2 nm in size). From the obtained results, $C_{26}H_{18}O$ can react readily with fullerene species in the gas phase, supporting the reaction of fullerene species with large molecules during the formation of dust particles.

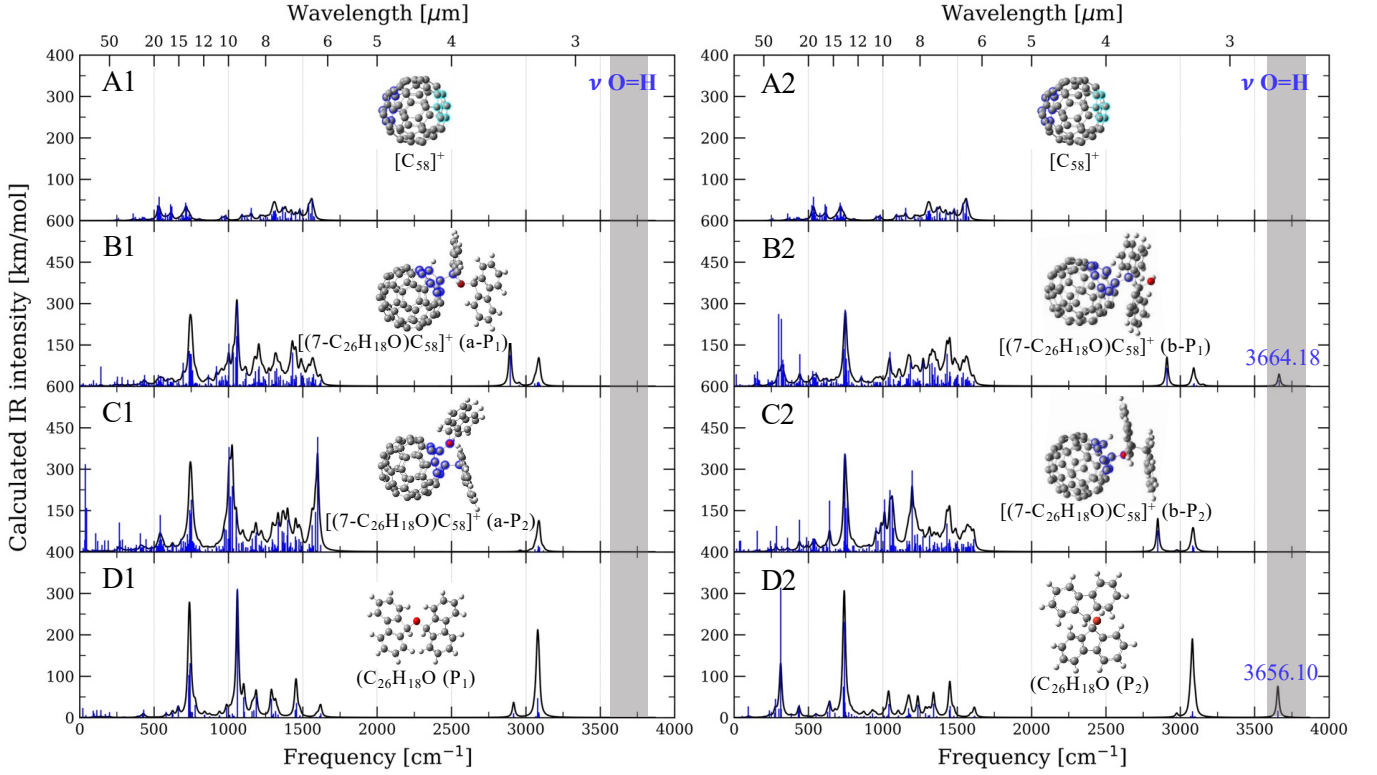


Figure 11. Computed IR spectra and vibrational normal modes for $C_{58}^+/C_{26}H_{18}O$ cluster cations: panels (A1–D1) are for $C_{58}^+ + C_{26}H_{18}O$ (P_1), and panels (A2–D2) for $C_{58}^+ + C_{26}H_{18}O$ (P_2), respectively. The vibrational band positions were scaled by 0.967 for C-H stretch mode and 0.980 for all other modes.

The newly formed fullerene/9-hydroxyfluorene cationic clusters may also be candidates for the observed IR interstellar bands. They may exist in the same interstellar area through an evolutionary ion-molecular reaction network between substituted PAHs and fullerenes. This may contribute to the observed interstellar spectrum and motivate spectroscopic studies (Tielens 2013).

Fig. 10 demonstrates the calculated IR spectra for some possible typical fullerene/9-hydroxyfluorene clusters: panels (A1 & A2) are for C_{60}^+ and C_{58}^+ , respectively; panels (B1–E1) for $[(C_{13}H_{10}O)C_{60}]^+$ (P_1 – P_4); panels (B2–E2) for $[(7-C_{13}H_{10}O)C_{58}]^+$ (P_1 – P_4); panels (F1 & F2) for $C_{13}H_{10}O$. Similarly, Fig. 11 demonstrates the calculated IR spectra for some possible typical $C_{58}^+/C_{26}H_{18}O$ clusters: panels (A1 & A2) are for C_{58}^+ ; panels (B1 & C1) for $[(C_{26}H_{18}O)C_{58}]^+$ (a- P_1 & a- P_2); panels (B2 & C2) for $[(C_{26}H_{18}O)C_{58}]^+$ (b- P_1 & b- P_2); panels (D1 & D2) for $C_{26}H_{18}O$ (P_1 & P_2). The vibrational band positions were scaled by a mode-dependent scaling factor, which is 0.967 for C-H stretch mode and 0.980 for all other modes (Bauschlicher & Langhoff 1997; Boersma et al. 2014), and the black line is the spectrum simulated by Gaussians with a full-width at half-maximum of 10 cm^{-1} .

As shown in Fig. 10 and Fig. 11, the IR spectra are very complex, in which many vibration modes are difficult to identify. In general, the IR spectra of fullerene/9-hydroxyfluorene derivate cluster cations were different from that of fullerene cations and $C_{13}H_{10}O$ or $C_{26}H_{18}O$. There are some new vibrational modes, some missing ones, and some reserved ones. The IR spectra with different binding modes are different in the peak positions and IR intensities. Different cage surfaces also contribute to different IR spectra, since the intensities of each vibrational peak are different in the spectra of $C_{58}^+/9$ -

hydroxyfluorene clusters on the 7 C-ring surfaces or $C_{60}^+/9$ -hydroxyfluorene clusters on the 6 C-ring surfaces.

We only conclude one characteristic peak in the range of $3500\text{--}3800\text{ cm}^{-1}$: the O-H stretch vibration. The O-H stretch features have been observed in space, especially in interstellar ices (e.g., Allamandola et al. 1992; Tielens et al. 1996). Since the cationic clusters in this study are relevant to planetary nebulae devoid of such ices, the O-H stretch vibrational mode in observations of planetary nebulae may be a reliable indicator of fullerene/9-hydroxyfluorene or similar clusters. The peak positions and intensities of the O-H stretch vibration change with different binding modes, which is shown in Fig. 10(B1–F1 & B2–F2) and Fig. 11(B1–D1 & B2–D2). For example, in Fig. 10(D1 & D2), with regard to the IR spectrum of $[(C_{13}H_{10}O)C_{60}]^+$ (P_3) and $[(C_{13}H_{10}O)C_{58}]^+$ (P_3), the characteristic peaks are 3689.64 and 3689.58 cm^{-1} , respectively; in Fig. 10(F1 & F2), concerning the IR spectrum of $C_{13}H_{10}O$, the characteristic peak of the O-H stretch vibration is 3702.69 cm^{-1} . We can see that for the clusters formed with the fracture of the O-H bond (e.g., $[(C_{13}H_{10}O)C_{58}]^+$ (P_4), $[(C_{26}H_{18}O)C_{58}]^+$ (a- P_1 , a- P_2 & b- P_2)), the O-H stretch vibration mode is missing. Interestingly, as for Van der Waals molecules with different alignments ($[(C_{13}H_{10}O)\dots C_{60}]^+$ (P_1 & P_2)), there is an obvious difference in the peak position and intensity of the O-H stretch vibration, while the peak position and intensity of other vibration modes are almost the same.

Overall, these calculated IR spectra reveal the complexity of fullerene/9-hydroxyfluorene cluster cations, which suggests the significant role of different geometric structures, including alignment, cage surface, and connection type. Due to the structure of fullerene/9-hydroxyfluorene clusters initially

formed being diverse, for deeply understanding the evolution of fullerene/PAH derivatives in cosmic environment, further observational and theoretical studies are necessary, such as more high-resolution observation data (e.g., the James Webb Space Telescope) or extensive theoretical calculations involving fullerenes (Berné et al. 2022; Barzaga et al. 2023; Lai et al. 2023; Xu et al. 2023; Yang & Li 2023).

6 CONCLUSIONS

Combining experiments with quantum chemical calculations, the reaction processes of fullerene cations with oxygenated functional PAH molecules are studied in this work. Fullerene/9-hydroxyfluorene cluster cations are efficiently formed through an ion-molecule collision reaction in the gas phase. Through theoretical quantum calculations, the molecular structures of newly formed clusters (e.g., $[(C_{13}H_{10}O)C_{60}]^+$, $[(C_{13}H_{10}O)_{1-2}C_{58}]^+$, and $[(C_{26}H_{18}O)C_{58}]^+$), the binding energies of their reaction pathways, together with their IR spectra, are obtained. Smaller fullerene cations have an enhanced chemical reactivity due to their deformed carbon rings (e.g., 7 C-ring). The bonding ability plays a decisive role in the cluster formation processes. Various factors that affect chemical reactivity differently are discussed, such as reaction surfaces, reaction modes, and combination sites.

The results we obtained once again validate the complexity of interstellar molecules and the diversity of the evolution for fullerene species under the constraints of coexisting PAH molecules. Hence, if these fullerenes are present in space, forming fullerene-based clusters could produce an extended family of large molecules. In addition, the results we obtained provide insights into interstellar chemistry of fullerene species and the geometry structures and functional groups that may affect the formation process of fullerene-PAH-derived cluster cations in the ISM.

ACKNOWLEDGEMENTS

This work is supported by the National Natural Science Foundation of China (NSFC, Grant No. 12333005, 12122302, and 12073027). Theoretical calculations were performed at the Supercomputing Center of the University of Science and Technology of China.

DATA AVAILABILITY

All data generated or analyzed during this study are included in this article.

REFERENCES

- Allamandola L., 2011, *EAS Publications Series*, 46, 305
 Allamandola L. J., Sandford S. A., Tielens A. G. G. M., Herbst T. M., 1992, *ApJ*, 399, 134
 Allamandola L. J., Tielens A. G. G. M., Barker J. R., 1989, *ApJS*, 71, 733
 Bakes E. L. O., Tielens A. G. G. M., 1994, *ApJ*, 427, 822
 Barzaga R., García-Hernández D. A., Díaz-Tendero S., Sadjadi S., Manchado A., Alcami M., Gómez-Muñoz M. A., Huertas-Roldán T., 2023, *ApJS*, 269, 26
 Bauschlicher C. W., Langhoff S. R., 1997, *Spectrochimica Acta Part A: Molecular Spectroscopy*, 53, 1225
 Becke A. D., 1992, *J. Chem. Phys.*, 96, 2155
 Berné O., et al., 2022, *PASP*, 134, 054301
 Bernstein M. P., Elsila J. E., Dworkin J. P., Sandford S. A., Allamandola L. J., Zare R. N., 2002, *ApJ*, 576, 1115
 Berné O., Tielens A. G. G. M., 2012, *PNAS*, 109, 401
 Boersma C., et al., 2014, *ApJS*, 211, 8
 Böhme D. K., 2016, *Phil. Trans. A Math. Phys. Eng. Sci.*, 374, 20150321
 Cami J., Bernard-Salas J., Peeters E., Malek S. E., 2010, *Science*, 329, 1180
 Campbell E. K., Maier J. P., 2018, *ApJ*, 858, 36
 Campbell E. K., Holz M., Gerlich D., Maier J. P., 2015, *Nature*, 523, 322
 Candian A., Gomes Rachid M., MacIsaac H., Staroverov V. N., Peeters E., Cami J., 2019, *MNRAS*, 485, 1137
 Cordiner M. A., et al., 2017, *ApJ*, 843, L2
 Cordiner M. A., et al., 2019, *ApJ*, 875, L28
 Doroshenko V. M., Cotter R. J., 1996, *Rapid communications in mass spectrometry*, 10, 65
 Dunk P. W., Adjizian J.-J., Kaiser N. K., Quinn J. P., Blakney G. T., Ewels C. P., Marshall A. G., Kroto H. W., 2013, *Proc. Natl. Acad. Sci.*, 110, 18081
 Frisch M. e., et al., 2016, *Gaussian 16*, revision C. 01
 García-Hernández D. A., Manchado A., García-Lario P., Stanghellini L., Villaver E., Shaw R. A., Szczerba R., Perea-Calderón J. V., 2010, *ApJ*, 724, L39
 García-Hernández D. A., Cataldo F., Manchado A., 2013, *MNRAS*, 434, 415
 Gavilan Marin L., Bejaoui S., Haggmark M., Svadlenak N., de Vries M., Sciamma-O'Brien E., Salama F., 2020, *ApJ*, 889, 101
 Grimme S., Ehrlich S., Goerigk L., 2011, *J. Comput. Chem.*, 32, 1456
 Hollenbach D. J., Tielens A. G. G. M., 1999, *Rev. Mod. Phys.*, 71, 173
 Hu X., Zhang D., Zhang C., Yang Y., Chen Y., Zhen J., Qin L., 2021a, *MNRAS*, 508, 4758
 Hu X., Zhang D., Yang Y., Chen Y., Qin L., Zhen J., 2021b, *ApJ*, 918, 81
 Hu X., Dong Z., Liu J., Zhen J., Qin L., 2023, *MNRAS*, 522, 4626
 Jäger C., Huisken F., Mutschke H., Jansa I. L., Henning T., 2009, *ApJ*, 696, 706
 Lai T. S. Y., et al., 2023, *ApJ*, 957, L26
 Le Page V., Snow T. P., Bierbaum V. M., 2001, *ApJS*, 132, 233
 Lee S. U., Han Y.-K., 2004, *The Journal of Chemical Physics*, 121, 3941
 Lee C., Yang W., Parr R. G., 1988, *Phys. Rev. B*, 37, 785
 Lifshitz C., 2000, *Int. J. Mass Spectrom.*, 200, 423
 McGuire B. A., et al., 2021, *Science*, 371, 1265
 Montillaud J., Joblin C., Toublanc D., 2013, *A&A*, 552, A15
 Omont A., 2016, *A&A*, 590, A52
 Petrie S., Bohme D. K., 1993, *Nature*, 365, 426
 Puget J. L., Leger A., 1989, *ARA&A*, 27, 161
 Sato S., Maeda Y., Guo J.-D., Yamada M., Mizorogi N., Nagase S., Akasaka T., 2013, *J. Am. Chem. Soc.*, 135, 5582
 Sellgren K., 1984, *ApJ*, 277, 623
 Sellgren K., Werner M. W., Ingalls J. G., Smith J. D. T., Carleton T. M., Joblin C., 2010, *ApJ*, 722, L54
 Tielens A., 2008, *ARA&A*, 46, 289
 Tielens A., 2013, *Rev. Mod. Phys.*, 85, 1021
 Tielens A. G. G. M., Wooden D. H., Allamandola L. J., Bregman J., Witteborn F. C., 1996, *ApJ*, 461, 210
 Walker G. A. H., Bohlender D. A., Maier J. P., Campbell E. K., 2015, *ApJ*, 812, L8

Xu J., Li A., Li X., Hou G.-L., 2023, MNRAS, 525, 3061
 Yang X., Li A., 2023, Nature, 621, 260
 Zhen J., Castellanos P., Paardekooper D. M., Linnartz H., Tielens A. G. G. M., 2014, ApJ, 797, L30
 Zhen J., Zhang W., Yang Y., Zhu Q., 2019a, MNRAS, 490, 3498
 Zhen J., Zhang W., Yang Y., Zhu Q., Tielens A. G. G. M., 2019b, ApJ, 887, 70

APPENDIX A: EXPERIMENTAL METHODS

The experiment was performed in the setup equipped with the quadrupole ion trap and a reflection time-of-flight (QIT-TOF) mass spectrometry. More detailed information is provided in Zhen et al. (2019b). Briefly, the fullerene molecule (C_{60}) was sublimated in an oven at a temperature of ~ 613 K and ionized by an electron gun (Jordan, C-950, ~ 82 eV). The fullerene cations of interest were then transported into the quadrupole ion trap (Jordan, C-1251) via an ion gate and a quadrupole mass filter (Ardara, Quad-925mm-01).

The gas-phase 9-hydroxyfluorene molecules were produced by heating their powder (J&K Scientific, with purity better than 99 %) in another oven (heating at ~ 380 K) mounted over the ion trap, which was effused continuously towards the center of the ion trap during the experiment. In the ion trap, fullerene/9-hydroxyfluorene cluster cations were formed through ion-molecule collision reactions between fullerene cations and 9-hydroxyfluorene molecules. Buffer gas helium with high purity was used to thermalize the ions through collision (~ 300 K). The pressures in the ion trap chamber were $\sim 6.0 \times 10^{-7}$ and $\sim 2.0 \times 10^{-7}$ mbar in the cases with and without adding 9-hydroxyfluorene molecules, respectively.

To generate a larger amount of photo-fragments of small fullerene ions, a third harmonic output (355 nm) of a Nd:YAG laser (Spectra-Physics, INDI, pulse width ~ 6 ns, frequency 10 Hz) was used to irradiate the trapped fullerene cations. Furthermore, to obtain detailed formation pathways of each fullerene cation, the stored waveform inverse Fourier transform excitation (SWIFT) isolation technique (Doroshenko & Cotter 1996) was introduced to the ion trap that allows to select the desired individual fullerene cations with specific mass/charge (m/z) range.

The whole set of experiments was conducted at a typically measured frequency of 0.1 Hz, i.e. each measurement period is 10 s. A high precision digital delay/pulse generator (SRS, DG535) was used to control the time sequence, which was set as follows:

- (1) Without SWIFT isolation: the ion gate kept open during the time interval 0–4.0 s, allowing C_{60}^+ to accumulate to a certain amount, and the beam shutter then kept open during 4.0–5.8 s, allowing trapped ions to be irradiated by a 355 nm laser beam. After the irradiation, the newly formed fullerene ions further reacted with 9-hydroxyfluorene molecules for several seconds. At 9.88 s, the ions were introduced out of the ion trap and then into a mass spectrometer to be detected;
- (2) With SWIFT isolation: the ion gate is kept open during the time interval 0–4.0 s, and the beam shutter is then kept open during 4.0–5.8 s. After the irradiation, a SWIFT isolation technique was employed to select the fullerene cations of interest (5.8–6.0 s). The selected ions then react with 9-hydroxyfluorene molecules for 3.88 s (6.0–9.88 s). At 9.88 s, the ions were introduced out of the ion trap and then into a mass spectrometer to be detected.

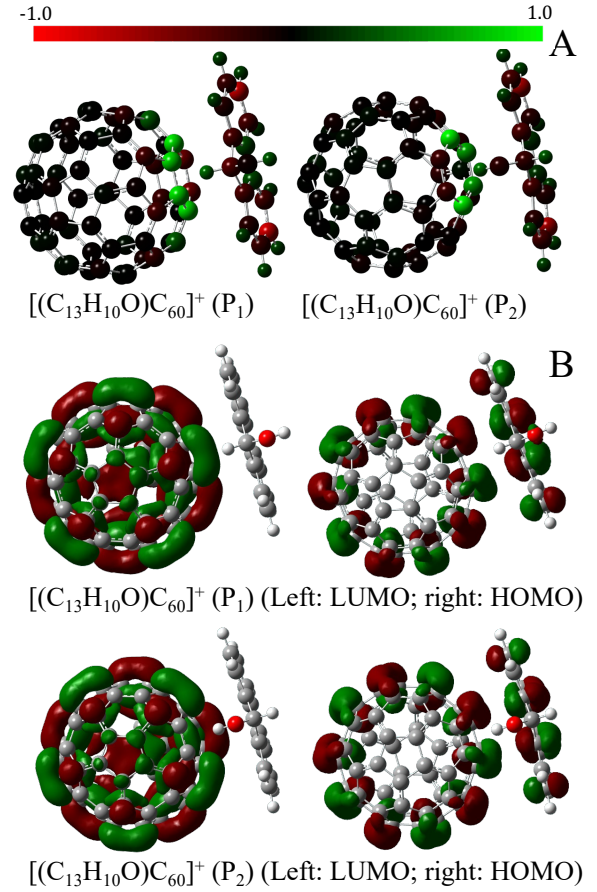


Figure B1. The 3D images of the Mulliken charge separation (A), the HOMO and LUMO (B) for Van der Waals molecules $[(C_{13}H_{10}O)\dots C_{60}]^+$ (P₁) and (P₂). In the Mulliken charge separation, atoms are colored according to charge. Red and green correspond to negative and positive electricity, respectively.

APPENDIX B: CHARGE POPULATION ANALYSIS

In Section 3, the formation of two different Van der Waals molecules $[(C_{13}H_{10}O)\dots C_{60}]^+$ (P₁) and (P₂) have almost the same exothermic energy of -0.82 eV (-18.9 kcal mol⁻¹). Here, we provided a Mulliken charge analysis performed by the Gaussian 16 program (Frisch et al. 2016) package, using density functional theory employing the hybrid functional B3LYP (Becke 1992; Lee et al. 1988) with the 6-311++G(d,p) basis set. We also visualized the HOMO and LUMO of these Van der Waals molecules, respectively.

Fig. B1 shows the 3D images of the Mulliken charge separation, the HOMO and LUMO for these two Van der Waals molecules $[(C_{13}H_{10}O)\dots C_{60}]^+$ (P₁) and (P₂), respectively. As demonstrated in Fig. B1, $[(C_{13}H_{10}O)\dots C_{60}]^+$ (P₁) and (P₂) have similar charge separation and orbital behavior, which implies similar stability of different Van der Waals molecules. During the formation of Van der Waals molecules, the cage surfaces of C_{60}^+ and the aromatic rings of $C_{13}H_{10}O$ are dominant and may be related to binding energy. We can see that there is only a small difference in electronegativity of O atoms between the two molecules. Therefore, we think the almost similar exothermic energy may be reliable, and different alignment may not affect significantly.